A discrete dislocation analysis of rate effects on mode I crack growth

Cleveringa, H.H.M.; van der Giessen, E.; Needleman, A.

Published in:
Materials science and engineering a-Structural materials properties microstructure and processing

DOI:
10.1016/S0921-5093(01)01177-7

Publication date:
2001

ELSEVIER

Materials Science and Engineering A317 (2001) 37–43

MATERIALS SCIENCE & ENGINEERING A

www.elsevier.com/locate/msea

A discrete dislocation analysis of rate effects on mode I crack growth

H.H.M. Cleveringa [a], E. Van der Giessen [a], A. Needleman [b,*]

[a] *Delft University of Technology, Koiter Institute Delft, Mekelweg 2, 2628 CD Delft, The Netherlands*
[b] *Division of Engineering, Brown University, Providence, RI 02912, USA*

Abstract

The mesoscopic growth of a crack in an elastic-plastic single crystal under mode I loading conditions is studied using a formulation involving discrete dislocation dynamics and cohesive surfaces. A two-dimensional analysis is carried out with the dislocations all of edge character and modeled as line singularities in an elastic material. At each stage of loading, superposition is used to represent the solution in terms of solutions for edge dislocations in a half-space and a complementary solution that enforces the boundary conditions. The latter is non-singular and obtained from a finite element solution. The lattice resistance to dislocation motion, dislocation nucleation, dislocation interaction with obstacles and dislocation annihilation are incorporated into the formulation through a set of constitutive rules. The cohesive surface methodology allows crack growth to emerge naturally from the boundary value problem solution. Material parameters representative of aluminum are employed. This study focuses on the influence of dislocation nucleation rate and loading rate on the course of crack growth.

Keywords: Mesoscopic; Dislocation; Fractive

1. Introduction

The interaction between discrete dislocations and crack tip fields has been the object of many studies, e.g. Weertman et al. [1], Lin and Thomson [2], Hirsch and Roberts [3], Shastry et al. [4], Zacharopoulos et al. [5] and Cleveringa et al. [6]. Although these studies address somewhat different issues or material characteristics and use different techniques, they show that dislocations play a dual role in the fracture process. On the one hand, dislocation activity gives rise to plastic dissipation that increases the crack growth resistance. On the other hand, the local stress concentration associated with discrete dislocations in the vicinity of the crack tip promote fracture.

This dual nature was made very explicit in the recent work of Cleveringa et al. [6], who carried out full boundary value problem solutions for small scale yielding of a mode I crack in plane strain. At each time step, the stresses and strains are written as superpositions of stress and deformation fields due to the discrete dislocations, which are singular inside the body and complimentary fields that enforce the boundary conditions and any continuity conditions across internal phase boundaries. Short-range dislocation interactions enter the formulation through constitutive rules for drag during dislocation motion, interactions with obstacles and dislocation nucleation and annihilation. The fracture properties of the material are specified in a cohesive surface constitutive relation. The plastic stress–strain response, the evolution of the dislocation structure, as well as crack initiation and crack growth, are all outcomes of the solution of the boundary value problem.

For a fixed loading rate, the fracture behavior in Ref. [6] was found to depend sensitively on the density of dislocation sources and obstacles. For a sufficiently low density of dislocation sources, only isolated dislocations were generated and crack propagation took place in a brittle manner. When ample nucleation sites were available, but the obstacle density was sufficiently low, the dislocations were found to strongly relax the near-tip

* Corresponding author. Tel.: +1-401-8632863; fax: +1-401-8631157.
E-mail address: needle@engin.brown.edu (A. Needleman).

0921-5093/01/$ - see front matter
PII: S0921-5093(01)01177-7

stresses, resulting in continued crack tip blunting without crack propagation. Between these two extremes, crack propagation with plastic dissipation took place.

In this paper, the same boundary value problem as in Ref. [6] is addressed, but the focus is on rate effects in the intermediate regime when crack propagation with plastic dissipation occurs. Three characteristic times enter the formulation: one associated with the rate of loading, one associated with the rate of dislocation nucleation and one associated with the mobility of dislocations. The characteristic times associated with the loading rate and with the rate of dislocation nucleation are varied, while keeping the characteristic time associated with dislocation mobility fixed.

2. Problem formulation and method of analysis

Symmetry about the crack plane and small scale yielding conditions are assumed. Attention is restricted to small strains, inertial effects are assumed negligible and the material is characterized in terms of a linear elastic constitutive relation. The analysis is limited to the 1000×500 μm region shown in Fig. 1, with plastic deformation confined to a process window which is taken to have dimensions $L_p = 10$ μm by $h_p = 12.5$ μm. The small-scale yielding conditions involve imposing displacements consistent with the elastic mode I singular field on the remote boundary of the region analyzed. A finite element mesh of 120×100 bilinear quadrilateral elements is used, with a high degree of refinement (80×80 elements) inside the process window.

Crack growth is modeled using a cohesive surface framework, where the fracture characteristics of the material are embedded in a traction–separation relation [7]. The cohesive constitutive relation for the normal traction T_n is taken to have the form of the exponential universal binding law [8]

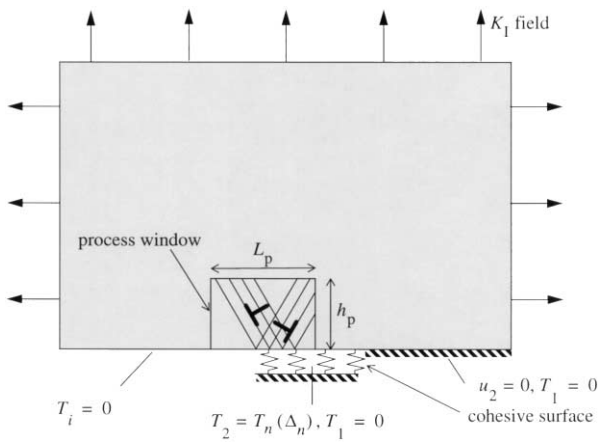

Fig. 1. Small-scale yielding analysis under mode I conditions with discrete dislocations moving inside a process window. Because of symmetry, only half the problem needs to be analyzed. A cohesive surface ahead of the initial crack is used to describe crack growth.

$$T_n(\Delta_n) = -\sigma_{max}\frac{\Delta_n}{\delta_n}\exp\left(-\frac{\Delta_n}{\delta_n}+1\right), \tag{1}$$

with Δ_n being the normal separation of the cohesive surface. The normal to the cohesive surface is parallel to the x_2-axis (Fig. 1) so that, with symmetry about $x_2 = 0$, the opening of the cohesive surface, Δ_n, is given by $\Delta_n = 2u_2(x_1, 0)$. In this study, the cohesive surface properties are taken to be $\sigma_{max} = 0.6$ GPa and $\delta_n = 4b$, giving a work of separation, $\phi_n = \exp(1)\sigma_{max}\delta_n$ of 1.63 J m^{-2}.

The dislocations are treated as line singularities in an elastically isotropic material, with Young's modulus $E = 70$ GPa and Poisson's ratio $\nu = 0.33$. Edge dislocations with Burger's vector $b = 0.25$ nm are considered on two slip systems that are symmetrically oriented at $\pm 60°$ to the crack plane. For each slip system there are 401 slip planes equally spaced over the process window, with a spacing of $86b$. Initially, these slip planes are assumed not to have any mobile dislocations, but to have a random distribution of dislocation sources and obstacles.

The computation of the deformation history is carried out in an incremental manner with a monotonically increasing value of the amplitude of the mode I crack tip field, K_I. Each time step involves three main computational stages: (i) determining the Peach–Koehler forces on the dislocations; (ii) determining the rate of change of the dislocation structure, caused by the motion of dislocations, the generation of new dislocations, their mutual annihilation and their possible pinning at obstacles; and (iii) determining the stress and strain state for the updated dislocation arrangement.

At a given stage of loading, the velocity, strain-rate and stress-rate fields are written as the superposition of two fields, for example:

$$\dot{\sigma}_{ij} = \tilde{\dot{\sigma}}_{ij} + \hat{\dot{\sigma}}_{ij}. \tag{2}$$

The ($\tilde{}$) fields are the fields of the individual dislocations in their current configuration and give rise to tractions $\tilde{T}_i$ and displacements $\tilde{U}_i$ on the boundary of the body. Here, the individual dislocation fields are those for an edge dislocation in a traction-free half-space, Freund [9], with the traction-free surface corresponding to the crack plane $x_2 = 0$. The ($\hat{}$) fields represent the image fields that correct for the actual boundary conditions. It may be shown [6] that these fields are governed by the rate of virtual work statement

$$\begin{aligned}\int_V \dot{\sigma}_{ij}\delta\varepsilon_{ij}\,\mathrm{d}V + \frac{1}{2}\int_{S_{coh}} k_n(\tilde{\Delta}_n^{(t+\Delta t)} + \hat{\Delta}_n^{(t)})\dot{\hat{\Delta}}_n\delta\Delta_n\,\mathrm{d}S \\ = -\frac{1}{\Delta t}\left[\int_V \hat{\sigma}_{ij}^{(t)}\delta\varepsilon_{ij}\,\mathrm{d}V \right. \\ \left. -\frac{1}{2}\int_{S_{coh}} T_n(\tilde{\Delta}_n^{(t+\Delta t)} + \hat{\Delta}_n^{(t)})\delta\Delta_n\,\mathrm{d}S\right]\end{aligned} \tag{3}$$

with S_{coh} the cohesive surface and

$$k_n = -\frac{\partial T_n}{\partial \Delta_n}. \quad (4)$$

Since the ($\hat{}$) fields are smooth in the region of interest, the rate boundary value problem in Eq. (3) is conveniently solved using a finite element method. Convergence issues related to solving for the ($\hat{}$) fields and a convergence study are presented in Ref. [13].

Assuming dislocation glide only, the variation in the potential energy of the body due to infinitesimal variations in the position of the Ith dislocation is governed by the Peach–Koehler force $f^{(I)}$ given by

$$f^{(I)} = n_i^{(I)}\left(\hat{\sigma}'_{ij} + \sum_{J \neq I} \sigma_{ij}^{(J)}\right) b_j^{(I)}, \quad (5)$$

with $n_i^{(I)}$ the slip plane normal, $b_i^{(I)}$ the Burger's vector of dislocation I and the stress deviator $\sigma'_{ij} = \sigma_{ij} - (\sigma_{kk}/3)\delta_{ij}$. The stress deviator can be used in Eq. (5) instead of σ_{ij} because the hydrostatic part of the stress, σ_{kk}, does not contribute to the Peach–Koehler force; since the Burger's vector lies in the slip plane and $n_i^{(I)}$ is normal to it, $n_i^{(I)}\, b_i^{(I)} = 0$. The direction of $f^{(I)}$ is in the slip plane and normal to the dislocation line. The Peach–Koehler force determines the evolution of the dislocation structure, accounting for glide, generation, annihilation and pinning at obstacles according to a set of rules that will be discussed subsequently.

Experimental studies, for example on Al [10,11], have shown that dislocation velocities are approximately proportional to the Peach–Koehler force over a wide range of stress. Hence, we express the magnitude of the glide velocity $v^{(I)}$ of dislocation I as

$$f^{(I)} = Bv^{(I)}. \quad (6)$$

The value $B = 10^{-4}$ Pa·s of the drag coefficient (the reciprocal of the dislocation mobility) is representative for aluminum [12]. As in Ref. [13], a cut-off velocity of 20 m s^{-1} is used which is low enough to be effective in allowing substantially increased time steps and high enough not to effect the results significantly.

New dislocation pairs are generated by simulating Frank–Read sources. In two dimensions, such sources are simulated by point sources that generate a dislocation dipole when the magnitude of the Peach–Koehler force at the source exceeds a critical value $\tau_{nuc}b$ during a period of time τ_{nuc}. The distance L_{nuc} between the dislocations is taken to be specified by

$$L_{nuc} = \frac{E}{4\pi(1-\nu^2)}\frac{b}{\tau_{nuc}}. \quad (7)$$

At this distance, the shear stress of one dislocation acting on the other is balanced by the slip plane shear stress τ_{nuc}. The strength of the dislocation sources is randomly chosen from a Gaussian distribution with mean strength $\bar{\tau}_{nuc} = 50$ MPa and Standard deviation $0.2\bar{\tau}_{nuc}$. From Eq. (7), the mean nucleation distance is $L_{nuc} = 125b$. The nucleation time is the two-dimensional analogue of the time it takes for a Frank–Read source to generate a new, isolated loop. To investigate the influence of this time scale, the value of τ_{nuc} for some of the computations is varied from 1/2 to 100 times the value used in Ref. [6].

Annihilation of two dislocations with opposite Burgers vector occurs when they are sufficiently close together. This is modeled by eliminating two dislocations when they are within a material-dependent, critical annihilation distance $L_e = 6b$ [12].

Obstacles to dislocation motion are modeled as fixed points on a slip plane. Such obstacles account for the effects of small precipitates or for dislocations on other slip systems in blocking slip. Pinned dislocations can only pass the obstacles when their Peach–Koehler force exceeds an obstacle dependent value $\tau_{obs}b$. All obstacles are taken to have the same strength $\tau_{obs} = 150$ MPa.

The above rules for dislocation evolution are constitutive assumptions intended to incorporate short-range effects at an atomic scale that an elasticity based discrete dislocation formulation cannot resolve. Short-range interactions between dislocations on different slip planes near their junction are not accounted for separately in this analysis; such dislocations only interact through their long-range elastic fields. We also mention that when a dislocation glides towards the open crack it disappears from the system, but leaves a displacement jump of $b/2$ across the slip plane (the displacement jump caused by its dipole counterpart, which remains in the material, ensures that a step of b is left at the surface).

Further details and additional references on the discrete dislocation formulation are given in Refs. [6] and [13].

3. Numerical results

Initially, there are no mobile dislocations on the potentially activated slip planes. A density of sources $\rho_{nuc} = 49$ μm^{-2} and a density of obstacles $\rho_{obs} = 98$ μm^{-2} in the process window are prescribed. Although the magnitude of these densities correspond to one of the cases in Ref. [6], the actual distribution of sources and obstacles is different. Because of this, the results for the reference calculation here are close to, but not identical, to those presented in Ref. [6].

For fracture without any dislocation activity, so that all energy released is consumed by the cohesive surface, unstable crack growth occurs at an applied stress intensity factor K_0 of (Ref. [14]),

$$K_0 = \sqrt{\frac{E\phi_n}{1-\nu^2}}. \quad (8)$$

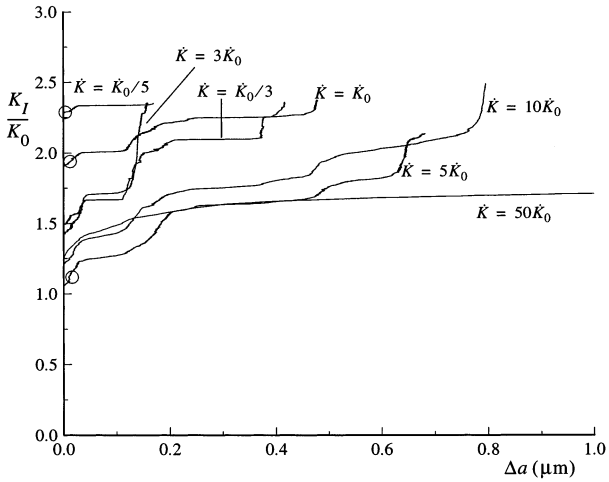

Fig. 2. Normalized applied stress intensity factor K_I/K_0 versus crack extension Δa for various loading rates. Dislocation distributions corresponding to the circles are shown in Fig. 3.

For the material parameters here $K_0 = 0.358$ MPa $\sqrt{\text{m}}$. The time it takes to reach K_0 is $K_0/\dot{K}_I$. If this time is less than the time to nucleate dislocations, then the material will remain elastic and brittle crack growth will occur. Cleveringa et al. [6] carried out calculations for an applied loading rate of $\dot{K}_0 = 50$ GPa$\sqrt{\text{m}}\,\text{s}^{-1}$, so that the characteristic time $t_0 = K_0/\dot{K}_0$ is $t_0 = 7.16$ μs. The time for dislocation nucleation used in Ref. [6] is denoted by t^0_{nuc} and is 0.01 μs. Here, we consider loading rates from $\dot{K}_0/5$ to 50 $\dot{K}_0$ and, hence, values of t_0 ranging from 35.8 to 0.143 μs; the values of t_{nuc} are taken to range from $t^0_{\text{nuc}}/2$ to 100 t^0_{nuc} (from 0.005 to 1 μs). These times can be compared with a characteristic time t_{m} associated with the mobility of dislocations, as governed by Eq. (6). Inserting the critical Peach–Koehler force for dislocation nucleation, $\bar{\tau}_{\text{nuc}}b$ and identifying this time with the time it takes for a dislocation to move over the average distance between obstacles, $\bar{s}_{\text{obs}}$, we have $t_{\text{m}} = B\bar{s}_{\text{obs}}/\bar{\tau}_{\text{nuc}}b$. For the parameters here ($\bar{s}_{\text{obs}} = 1/\sqrt{\rho_{\text{obs}}} \approx 0.1$ μm), $t_{\text{m}} = 0.0008$ μs. Since the corresponding average velocity of $\bar{s}_{\text{obs}}/t_{\text{m}} \approx 125$ m s^{-1} between obstacles is about six times larger than the cut-off velocity used in the computations, the actual characteristic time will be ≈ 0.005 μs.

Fig. 2 shows crack growth resistance curves obtained for the various loading rates and with the nucleation time equal to the reference value t^0_{nuc}. Here, the crack location used to compute the crack extension Δa is defined as the point along the cohesive surface, where the opening of the cohesive surface, Δ_{n}, is $2\delta_{\text{n}}$. As observed also in Ref. [6], crack initiation is quite sensitive to statistical effects, so that the various resistance curves do not order completely. However, there is a clear tendency that the resistance decreases with increasing loading rate. For the highest loading rate, $\dot{K}_I = 50\,\dot{K}_0$, there is virtually no increase in resistance once the crack has initiated, indicating that there is insufficient time for dislocation activity to effectively shield the crack tip. For the lower loading rates, crack growth takes place in 'spurts' of relatively brittle growth separated by periods in which the resistance increases significantly. This is caused by the fact that tangles of dislocations form in front of the crack tip which tend to arrest the crack and lead to dislocation motion and generation [6]. The results in Fig. 2 suggest that the spurts are shorter for lower loading rates, although this trend is blurred by statistical effects. Apparently, at the lower loading rates, there is more time available for dislocation tangles to form as the crack approaches.

Fig. 3 illustrates the dislocation distributions at the instant of crack growth initiation for three different loading rates. The values of K_I correspond to the circles in Fig. 2. For $\dot{K}_I = \dot{K}_0/5$, Fig. 3(a), a high dislocation density has developed, leading to substantial crack tip blunting. Nevertheless, the local stress state immediately near the tip is such that the crack starts to propagate at this instant. As explained in detail by Cleveringa et al. [6], this phenomenon is caused by the dual role played by dislocations. At the reference loading rate of $\dot{K}_0$ shown in Fig. 3(b), the overall dislocation density is much lower. In accordance with the lower value of K_I at the initiation of crack growth, the plastic zone, the region formed by the envelope around all dislocations, is smaller than in Fig. 3(a). In fact, the plastic zone sizes in Fig. 3 scale with the value of K_I^2, which is the scaling in conventional continuum plasticity. However, sufficiently close to the crack tip, the dislocation densities appear to be similar. At $\dot{K}_I = 5\dot{K}_0$, Fig. 3(c), there are rather few dislocations available to blunt the crack tip and, indeed, crack initiation occurs at a value of K_I, which is just slightly larger than K_0. At this loading rate, and even more so at $\dot{K}_I = 50\dot{K}_0$, the stress distribution near the tip (not shown) reveals that the elastic singular stress field is only partly relaxed by the dislocation shielding. It is also worth noting that these dislocation distributions give rise to a stress distribution away from the crack tip, that on average is very much like that given by the continuum slip analysis of Rice [15], while near the crack tip, discrete dislocation effects lead to substantially increased stress levels, see Ref. [6].

Although we see, as expected, that the dislocation density at the initiation of crack growth decreases with increasing loading rate, the dislocation density as a function of K_I during crack propagation appears to be almost independent of loading rate, as shown in Fig. 4. Here, the dislocation density ρ is defined as the number of dislocations divided by the area of the process window. Examination of the dependence of dislocation density on K_I shows that the dislocation density ρ increases as K_I^3 for all loading rates considered. The

origin of this power law behavior is not clear; Zacharopoulos et al. [5] observed that the number of dislocations increased roughly as $K_{III}^{5/3}$ in their mode III study, where dislocation nucleation only took place from the crack tip. The fact that the evolution of the dislocation density is seen to be independent of the loading rate indicates that even at the highest loading rates, there is ample time for the nucleation of dislocations. This is consistent with the fact that the shortest characteristic loading time of $t_0 = 0.143$ μs is still an order of magnitude larger than the nucleation time $t^0_{nuc} = 0.01$ μs.

The influence of the time needed to nucleate a dislocation dipole is investigated in Fig. 5. Apart from statistical variations in the instant at which crack growth initiates, this figure shows a tendency for longer nucleation times to reduce the resistance to crack growth. In particular, when $t_{nuc} = 100\ t^0_{nuc} = 1$ μs, while $t_0 = K_0/\dot{K}_0 = 7.16$ μs, there is time for dislocation activity prior to crack growth initiation, but once the crack begins to propagate, the nucleation time is too long to generate the dislocations needed to shield the crack tip. For values of $t_{nuc} = 4t^0_{nuc}$ and smaller, the average slope

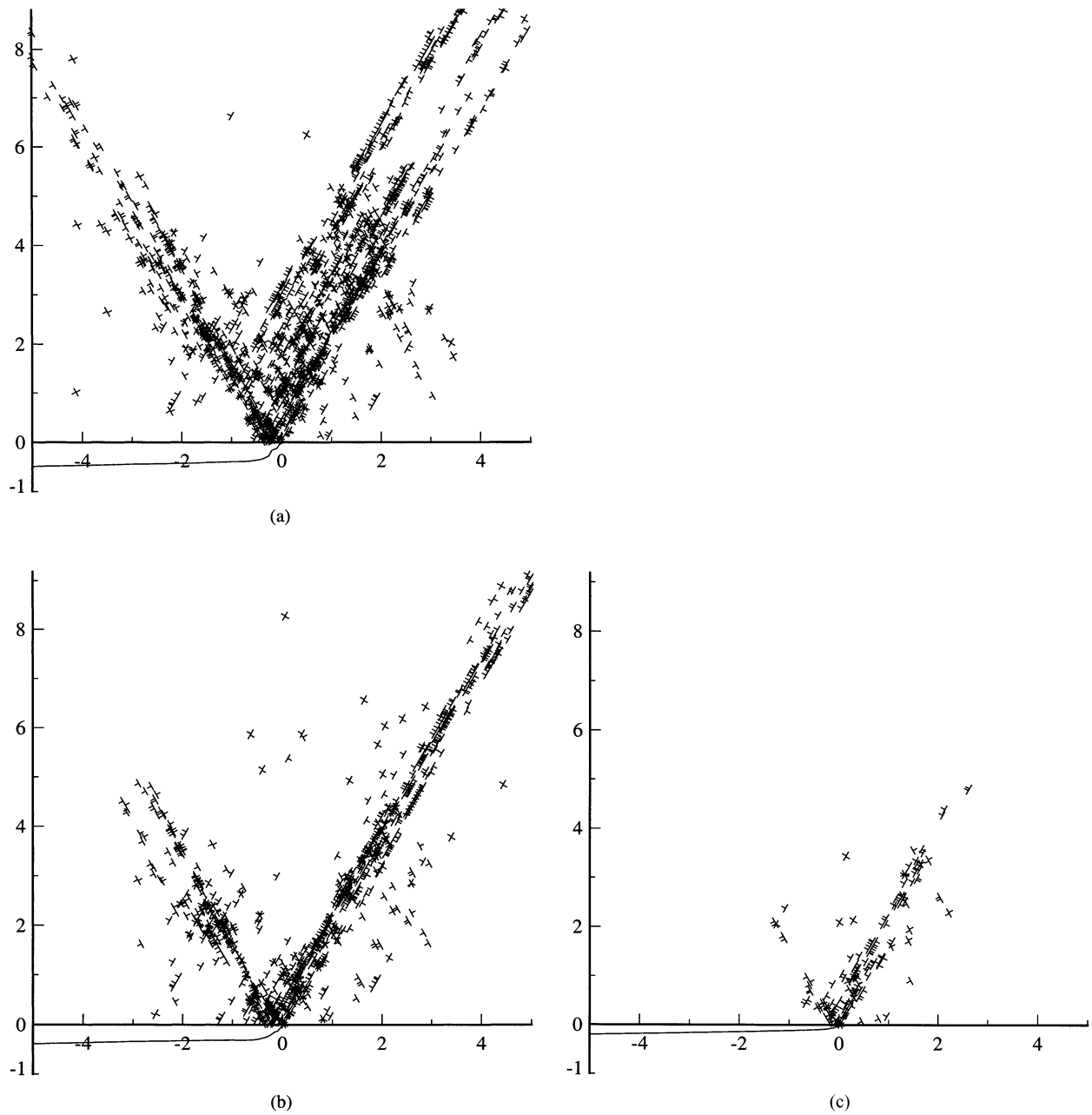

Fig. 3. Dislocation distributions inside a 10×9 μm section of the process window at crack initiation (cf. Fig. 2) for loading rates $\dot{K}_I$ of: (a) $\dot{K}_0/5$; (b) $\dot{K}_0$; (c) $5\dot{K}_0$. The corresponding crack opening profiles (displacements magnified by a factor of 10) are plotted below the x_1-axis.

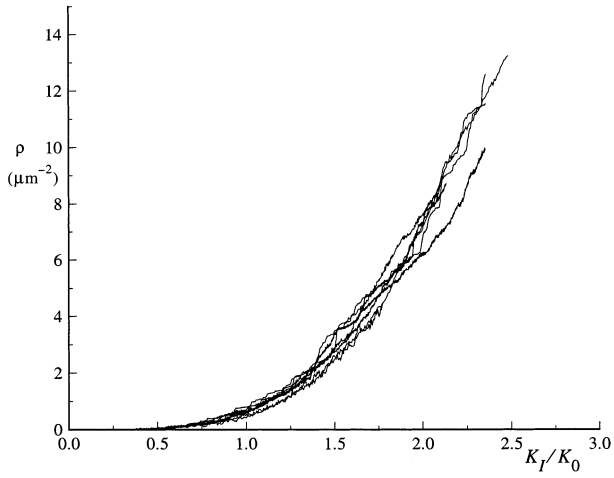

Fig. 4. Dislocation density measured over the entire process window versus the normalized applied stress intensity factor K_I/K_0 for the loading rates considered in Fig. 2.

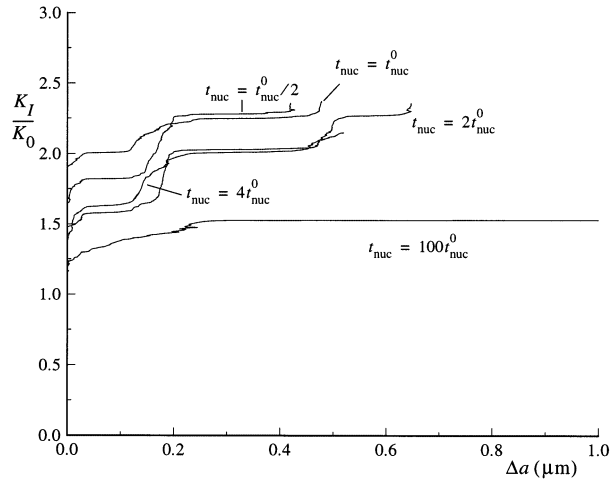

Fig. 5. Normalized applied stress intensity factor K_I/K_0 versus crack extension Δa for various nucleation rates.

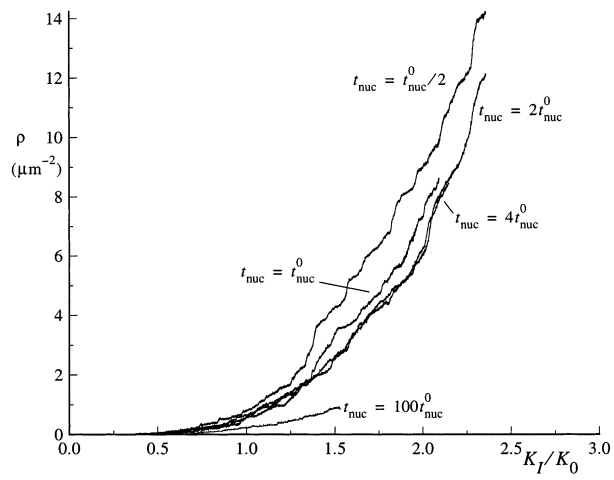

Fig. 6. Dislocation density measured over the entire process window versus the normalized applied stress intensity factor K_I/K_0 for the nucleation rates considered in Fig. 5.

of the K_I versus Δa curves is not very sensitive to the nucleation time. This suggests that, in these cases, this slope is controlled mostly by the mobility of dislocations relative to the loading rate, which is consistent with the findings in Fig. 2. The evolution of the dislocation density with K_I/K_0 in Fig. 6 for nucleation rates in the range between t^0_{nuc} and $4t^0_{nuc}$ essentially coincides with the curves in Fig. 4. Apparently, even for $t_{nuc} = 4t^0_{nuc}$, nucleation occurs quickly enough to generate the required number of dislocations. However, the case with $t_{nuc} = t^0_{nuc}/2$, where nucleation is faster than in the reference case, has a somewhat higher dislocation density. In this case, sources available in the material are more easily triggered by the high stress fields caused by passing dislocations. This leads to a high density of dislocations in the plastic zone above the crack, but these dislocations are sufficiently far from the tip that they do not substantially enhance the opening stress on the cohesive surface. For $t_{nuc} = 100t^0_{nuc}$, the dislocation density is significantly reduced, with dislocation nucleation being the rate limiting process.

4. Concluding remarks

The effects of loading rate and dislocation nucleation rate on the initiation and growth of a mode I crack have been analyzed using a framework where the interplay between plastic dissipation and material separation is an outcome of the boundary value problem solution. The fracture properties of the material are embedded in a cohesive surface constitutive relation and plastic flow arises from the collective motion of discrete dislocations.

A main focus in previous studies has been on initially dislocation-free materials, where dislocations are nucleated from the crack tip, e.g. Refs. [3,16]. However, there are circumstances where pre-existing dislocations have an important influence on the fracture toughness, as discussed in Ashby and Embury [17]. The focus here and in Ref. [6] is on materials where initially present dislocations may serve either as bulk sources for dislocation generation or as obstacles to dislocation motion. We find that, for the range of rates considered, the crack growth resistance is mainly controlled by the time scales of the nucleation and mobility of dislocations relative to that of the loading. For a high enough loading rate, there is insufficient time for dislocation activity to effectively shield the crack and crack propagation occurs in a brittle fashion. The crack growth resistance tends to increase with decreasing loading rate, although the general trend can be modified by statistical effects.

Acknowledgements

The work of H.H.M. Cleveringa is part of the research program of the 'Stichting voor Fundamenteel Onderzoek der Materie (FOM)' which is supported financially by the 'Nederlandse Organisatie voor Wetenschappelijk Onderzoek (NWO).' A. Needleman and E. Van der Giessen acknowledge support from the Materials Research Science and Engineering Center on On Micro- and Nano-Mechanics of Materials at Brown University (NSF Grant DMR-007-9964).

References

[1] J. Weertman, I.H. Lin, R. Thomson, Acta Metall. 31 (1983) 473–482.
[2] I.-H. Lin, R. Thomson, Acta Metall. 34 (1986) 187–206.
[3] P.B. Hirsch, S.G. Roberts, Scr. Metall. 23 (1989) 925–930.
[4] V. Shastry, P.M. Anderson, R. Thomson, J. Mater. Res. 9 (1994) 1–16.
[5] N. Zacharopoulos, D.J. Srolovitz, R. LeSar, Acta Mater. 45 (1997) 3745–3763.
[6] H.H.M. Cleveringa, E. Van der Giessen, A. Needleman, J. Mech. Phys. Solids 48 (2000) 1133–1157.
[7] A. Needleman, J. Appl. Mech. 54 (1987) 525–531.
[8] J.H. Rose, J. Ferrante, J. Smith, Phys. Rev. Lett. 47 (1981) 675–678.
[9] L.B. Freund, Adv. Appl. Mech. 30 (1994) 1–66.
[10] J.A. Gorman, D.S. Wood, T. Vreeland Jr, J. Appl. Phys. 40 (1969) 833–841.
[11] V.R. Parameswaran, N. Urabe, J. Weertman, J. Appl. Phys. 43 (1972) 2982–2986.
[12] L.P. Kubin, G. Canova, M. Condat, B. Devincre, V. Pontikis, Y. Bréchet, Sol. State Phenom. 2324 (1992) 455–472.
[13] H.H.M. Cleveringa, E. Van der Giessen, A. Needleman, Int. J. Plast. 15 (1999) 837–868.
[14] J.R. Rice, J. Appl. Mech. 35 (1968) 379–386.
[15] J.R. Rice, Mech. Mat. 6 (1987) 317–335.
[16] V.R. Nitzsche, K.J. Hsia, Mat. Sci. Eng. A176 (1994) 155–164.
[17] M.F. Ashby, J.D. Embury, Scr. Metall. 19 (1985) 557–562.